*Transactions*, SMiRT-24
BEXCO, Busan, Korea - August 20-25, 2017
Division II

# PERFORMANCE BASED FLAW TOLERANCE CONCEPT FOR FATIGUE DAMAGE ASSESSMENT OF AGED NUCLEAR POWER PLANTS

**Masayuki Kamaya**[1]

[1] Institute of Nuclear Safety System, Inc., Japan

## ABSTRACT

According to the flaw tolerance assessment, fatigue damaged components can be used even if the cumulative usage factor (CUF) equals 1 when no crack is found by inspection. The interval before the next inspection is determined by crack growth prediction. In most cases, fatigue damage assessment is conservative and the degree of the conservativeness can be deduced from the operating experience, that is, the fact there is no crack for the component with CUF = 1. In this study, a concept performance based flaw tolerance (PFT) was proposed to take the operating experience into account for the future crack growth prediction. Longer operating time and less crack growth secure a longer interval before the next inspection. To apply the PFT concept, first, the fatigue assessment using the CUF was replaced with the crack growth analysis. The allowable number of cycles prescribed by the design fatigue curve was successfully predicted by the crack growth assuming an initial depth of $a_i$ = 0.3 mm and accelerated growth rate corresponding to a structural margin. Then, the postulated crack growth curve (P-curve) was derived for the uniform and thermal loading conditions. The interval before the next inspection could be determined by the P-curve based on the operating time before the inspection, detectable crack size of the inspection technique and critical size for component failure. It was shown the PFT concept was also applicable to fatigue assessment in the pressurized water reactor coolant environment.

## INTRODUCTION

In the design of nuclear power plant components, fatigue damage is considered so that accumulated fatigue damage, which is quantified by the cumulative usage factor (CUF), does not exceed a critical value, that is, CUF = 1. The actual CUF accumulated during plant operation tends to be larger than that expected in the component design due to long term operation, environmental effect and consideration of large seismic loads. It has been said that the current fatigue damage assessment procedure is conservative and, to the author's knowledge, no cracks have been found at any location where fatigue damage was assessed in a component design. Therefore, it is deduced that no crack is found even if the actual CUF exceeds the critical value. According to a flaw tolerance assessment procedure such as the ASME Boiler and Pressure Vessel Code Section XI Appendix L (Gosselin et al., 2007), even if the CUF exceeds unity, the component can be used when no crack is found by inspection (Gilman et al., 2015). The allowable operating period is determined by crack growth prediction and the critical crack size for the crack growth determined by the fitness-for-service (FFS) assessment procedure (ASME, 2015a).

The primary parameters used in the fatigue damage assessment are fatigue damage driving force and the number of cycles. The main source of fatigue damage driving force is strain fluctuation caused by changes in the operating mode such as plant start-up and shutdown (Nakamura et al., 2007). Water temperature transient induces strain fluctuations on the component surfaces and fatigue damage. Then, the CUF is calculated using the allowable number of cycles given by the design fatigue curve and the number of cycles of strain fluctuations expected during plant operation. The CUF is calculated not only for the component design but also for operating plants in order to secure component integrity for long term operation. In the CUF calculation for operating plants, the strain amplitude is obtained in the same way as

Table 1: Fatigue damage assessments for design and operation phases

| | Design phase | Operation phase (current approach) | Operation phase (PFT) |
|---|---|---|---|
| Strain amplitude | Calculation | Calculation | Actual |
| Number of cycles | Design requirement | Actual | Actual |

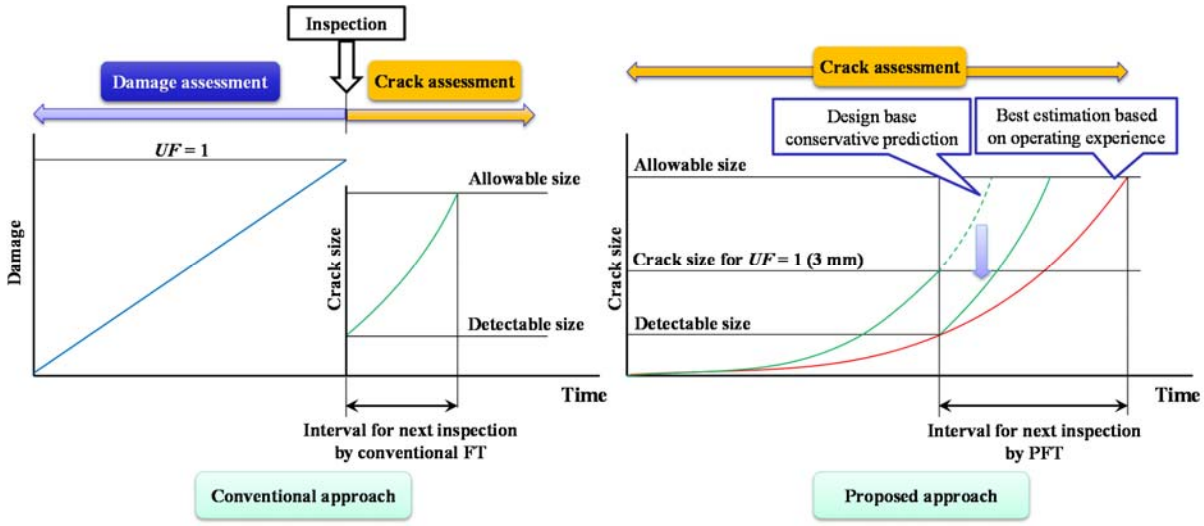


Figure 1. A schematic drawing representing the fatigue assessment procedure for design, operation and flaw tolerance. The crack growth assessment is applied to all phases in the PFT concept.

done for the component design and both are summarized in Table 1. Although some implementations have been applied to monitor the temperature and strain transients during plant operation (Rothenhöfer and Manke, 2013), in most cases, the amplitude of the strain fluctuations is determined by calculations for the conditions postulated in the plant design even in the operation phase. On the other hand, the actual number of cycles of strain fluctuations is counted in the operation phase whereas that given in design conditions is used in the design phase. Since the calculation of strain amplitude is generally conservative, the calculated CUF in the operation phase tends to be conservative. This conservative strain amplitude is also used in the flaw tolerance assessment.

In this study, in order to achieve a reasonable flaw tolerance assessment by eliminating the conservativeness in the strain assessment, the performance based flaw tolerance (PFT) concept is proposed. The conservative strain amplitude is corrected using operating experience. The fact that no crack is found in the component of CUF = 1 implies that the fatigue damage driving force is not as large as that estimated in the plant design. This fact is considered in the crack growth prediction in the PFT concept. In order to apply the PFT concept, the current fatigue assessment procedure using the CUF was transformed to that based on crack growth prediction. As schematically shown in Figure 1, the fatigue damage is assessed using the CUF in design and operation phases whereas the crack growth prediction is applied in the flaw tolerance assessment. Since the CUF is a conceptual parameter, it is difficult to determine the CUF value of an actual component. For example, it is difficult to say what the CUF value is for a component which has a 1 mm deep fatigue crack. Also, it is not clear what happens when the realistic CUF reaches the critical value. In a previous study using stainless steel (Kamaya and Kawakubo, 2012a), it was found that the incubation period before initiation of a small crack, with a length less than 20 micrometres, was negligibly small compared with the total fatigue life. The fatigue life could be predicted as the number of cycles necessary for the small crack to grow to a critical size for specimen failure. By applying crack growth assessment, it is possible to identify the degree of fatigue damage from the crack size. Moreover, even when no crack is

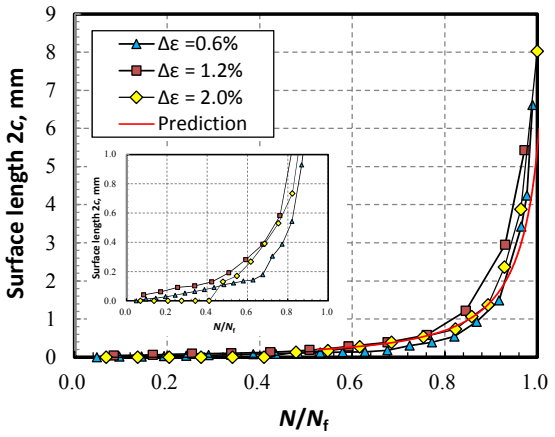


Figure 2. Changes in crack surface length obtained by strain-controlled fatigue tests and that obtained by crack growth prediction assuming initial depth of 50 μm.

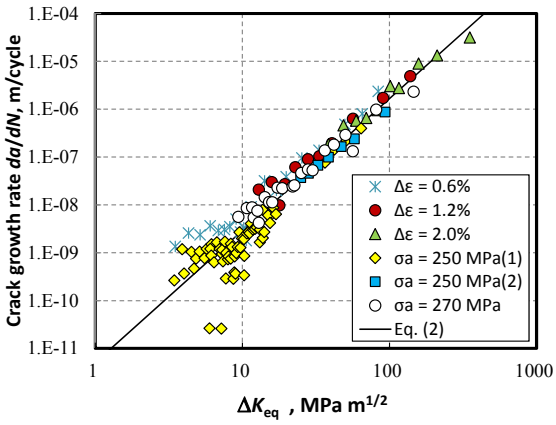


Figure 3. Relationship between the equivalent stress intensify factor range ($\Delta K_{eq}$) and crack growth rate obtained for various loading conditions.

found by inspection, possible fatigue damage can be estimated from the detection capability of the inspection technique. Then, by using the identified fatigue damage and the number of cycles, the fatigue damage driving force can be estimated.

In this paper, first, the basic idea of the fatigue assessment by the crack growth prediction was reviewed. Second, the PFT concept was proposed. Then, the PFT concept was applied to assess the fatigue damage accumulated in a pipe subjected to cyclic thermal loading. Finally, applicability of the PFT concept to the fatigue assessment in the pressurized water reactor (PWR) coolant environment was discussed.

## FATIGUE ASSESSMENT BY CRACK GROWTH PREDICTION

In order to obtain a correlation between crack size and degree of fatigue damage, crack initiation and growth behaviors were observed during fatigue tests using solution heat-treated Type 316 stainless steel in a room temperature laboratory environment (Kamaya, 2017). The tests were conducted for round-bar specimens of 10 mm diameter using a controlled strain range $\Delta\varepsilon$ of 0.6%, 1.2% or 2.0%. The numbers of cycles to failure (fatigue life) $N_f$ were 41,500, 5,937 and 1,495 cycles, respectively.

Changes in length on the specimen surface of the primary crack, which caused specimen failure, were obtained by periodical replica investigations as shown in Figure 2. The number of cycles was normalized by the fatigue life $N/N_f$. The cracks were observed at a relatively early stage of the fatigue tests and grew continuously. The initial crack lengths were 12.5 μm, 41.2 μm and 130.6 μm for $\Delta\varepsilon$ = 0.6%, 1.2% and 2.0%, respectively. These cracks were observed at $N/N_f$ = 0.096, 0.085 and 0.478, respectively. The surface roughness was enhanced for a relatively large strain range and that made it difficult to observe small cracks for $\Delta\varepsilon$ = 2.0%. It was concluded that the incubation period before crack initiation was relatively short: less than $N/N_f < 0.1$. The primary cracks grew without retardation and no coalescence was observed.

The crack growth rates were identified from the slope of each segment connecting adjacent points of the lines shown in Figure 2. The growth rate to the depth direction $da/dN$ was obtained by assuming the ratio of the depth $a$ to the surface length $2c$ to be $a/2c$ = 0.5 (Kamaya, 2013a). Figure 3 shows the relationship between the crack growth rates $da/dN$ and the equivalent stress intensity factor ($\Delta K_{eq}$), which is defined by (Kamaya and Nakamura, 2013):

$$\Delta K_{eq} = f \Delta\varepsilon E_{(25°C)} \sqrt{\pi a} \tag{1}$$

where $E_{(25°C)}$ is Young's modulus at 25°C and $E_{(25°C)}$ = 195 GPa was used. The geometrical correction factor $f$ was obtained by Kamaya and Kawakubo (2012b). $\Delta\varepsilon E_{(25°C)}$ is equivalent to the stress intensity used for

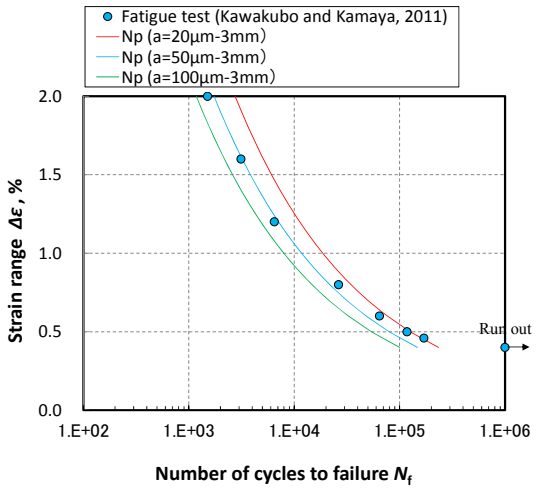


Figure. 4 Fatigue lives estimated by crack growth prediction and those obtained by the low-cycle fatigue tests.

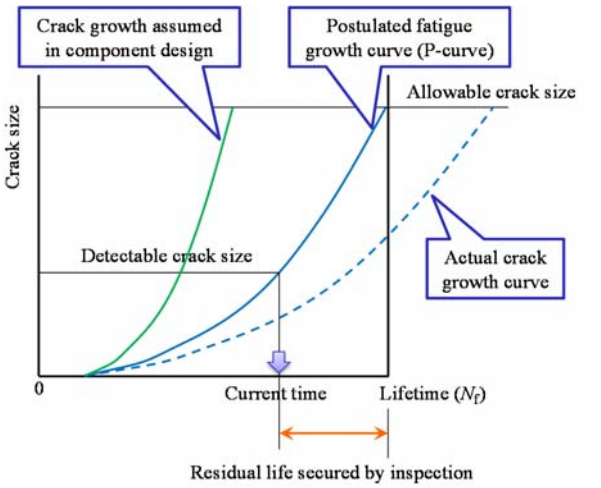


Figure 5. Schematic drawing representing the determination of crack growth curve by inspection results.

the ordinate of the design fatigue curve (ASME, 2015b). If no inelastic strain is included in $\Delta\varepsilon$, the $\Delta K_{eq}$ is equal to the stress intensity factor. The crack growth rates obtained for various loading conditions (Kamaya and Kawakubo, 2012a) including those obtained from Figure 2 seemed to be represented by a single curve. It has been shown that the fatigue life of stainless steel correlated better with the strain range than with the stress range (Jaske and O'Donnell,1977; Colin and Fatemi, 2010; Kamaya and Kawakubo, 2015). The fatigue life for component design is prescribed for the strain range (ASME, 2015b; Chopra and Shack, 2007). Since the fatigue life corresponded to the number of cycles for the small crack growing to the critical size and the fatigue life correlated well with the strain range, it is reasonable for the crack growth driving force to be represented by the parameter using the strain range. The good correlation in the growth rate and $\Delta K_{eq}$ implies that the driving force for growth can be represented by the $\Delta K_{eq}$ regardless of high- and low-cycle fatigue regimes. The regression of all data shown in Figure 3 has been obtained by Kamaya (2017) as:

$$\frac{da}{dN}\left[\mathrm{m/cycle}\right] = 5.06\times10^{-12}\left(\Delta K_{eq}\left[\mathrm{MPa}\sqrt{\mathrm{m}}\right]\right)^{2.76} \quad (2)$$

It should be noted that fatigue crack growth for the so-called small scale yielding condition also can be predicted by Equation 2 using stress intensity factor instead of $\Delta K_{eq}$.

The results shown in Figure 2 demonstrated that the fatigue life almost corresponded to the number of cycles for a small crack growing to a critical size for specimen failure. The critical size was about 3 mm in depth (Kamaya, 2013a). Then, the number of cycles was calculated for a small crack growing to 3 mm in depth. The initial crack depth $a_i$ was set to 20 μm, 50 μm or 100 μm. The growth rate was calculated using Equation 2 for a given strain range. The obtained number of cycles, which is denoted as $N_p$, and fatigue lives obtained by the strain-controlled fatigue test using the same material (Kawakubo and Kamaya, 2011) are compared in Figure 4. The growth prediction with $a_i$ = 50 μm was in good agreement with the fatigue life obtained by the fatigue tests except the high-cycle regime near the fatigue limit. The fatigue life treated in component design mainly belongs to the low-cycle fatigue regime. Thus, the damage assessment using CUF can be replaced by the crack growth prediction.

The change in crack length with the normalized fatigue life obtained by the growth prediction is indicated by the red line in Figure 2. It should be noted that the curve did not depend on the applied strain range. The obtained curve agreed well with the test results. By using the curve shown in Figure 2, it is possible to estimate the CUF from the crack length identified by inspection. If a 2 mm length crack is detected, the residual life is deduced to be less than $0.1N_f$.

Table 2: Subfactors considered in fatigue life of stainless steels.

| Factors | Margin | | | |
|---|---|---|---|---|
| | Chopra and Shack (2007) | | Initiation | Growth |
| | Variation | Log mean | | |
| Material variability and data scatter | 2.1-2.8 | 2.4 | $(2.4)^{0.5}$ | $(2.4)^{0.5}$ |
| Size effect | 1.2-1.4 | 1.3 | 1.3 | 1 |
| Surface finish | 2.0-3.5 | 2.6 | 2.6 | 1 |
| Loading history | 1.2-2.0 | 1.5 | 1 | 1.5 |
| Total | | ≅12 | ≅5 | ≅2.4 |

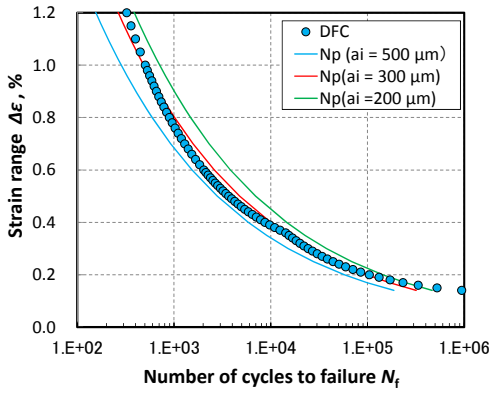


Figure 6 Prediction of DFC by crack growth prediction for various initial depth $a_i$ values

## PERFORMANCE BASED FLAW TOLERANCE CONCEPT

It is expected that no crack is found by inspection for components of CUF =1 because the current fatigue damage assessment is conservative. Since the design fatigue curve was determined using fatigue life obtained for small specimens, a 3 mm deep crack would be found if the realistic CUF reaches unity. The fact that no crack is found by an inspection with the detection capability less than 3 mm implies that the realistic CUF does not reach the critical value. This means that the strain amplitude is not as large as that estimated in component design. In the PFT concept, the future crack growth is predicted based on operating experience, that is, no crack is found by the inspection. From the inspection result, a possible crack growth curve can be deduced as schematically shown in Figure 5. Although actual crack size is not identified by the inspection, the maximum crack size can be determined from the detectability of the inspection technique applied. Then, it is possible to draw a crack growth curve so that the curve paths through the detectable crack size and current time. This curve is referred to as the postulated fatigue crack growth curve (P-curve) (Kamaya and Nakamura, 2013) in this study. Crack growth during future operation is deduced from the P-curve.

The above discussion was made based on the fatigue test results. On the other hand, the fatigue damage is assessed using the design fatigue curve (DFC) which includes various structural factors and safety margins. Therefore, the crack growth prediction using the growth rate obtained by the fatigue tests does not directly correspond to the CUF. The DFC of stainless steels is drawn by considering margins for effects of data scatter, component size, surface finish, loading history and so on. Details of the factors are given in Table 2 (Chopra and Shack, 2007). Chopra and Shack (2007) concluded that the DFC should be drawn by reducing the best-fit regression by a factor of 2 on stress (strain) and by 12 on cycles, whichever is more conservative. In order to estimate the DFC by the crack growth prediction, these margins of 2 and 12 have to be assigned to the crack initiation (initial size) and growth rate. Then, in the author's previous study (Kamaya, 2017), the margins for crack initiation and growth were determined as follows. Since the surface finish affects the incubation period or initial crack size and has little influence on the crack growth, the margin for the surface finish should be considered for the initiation. The size effect was also assigned to the initiation because the effect was considered for incorporating the difference in the risk volume for crack initiation. The chance of a larger crack initiation is deduced to be larger for actual components than the small specimens used in fatigue tests. On the other hand, the loading history effect was assigned to the growth because it takes account of the change in growth rate due to variable loading and the influence of growth for a small strain range less than the fatigue limit. The material variability and data scatter were considered for both initiation and growth. Then, as summarized in Table 2, the factor of 12 was divided into 5 for initiation and 2.4 for growth.

Table 3: Constants of stainless steel used for thermal stress analyses.

| | |
|---|---|
| Density × Specific heat: $c\rho$ | 3.85 $10^6$ [J/m$^3$K] |
| Heat conduction coefficient: $\lambda$ | 15.86 [W/mK] |
| Young's modulus: $E$ | 195000 [MPa] |
| Poison's ratio: $\nu$ | 0.3 |
| Heat expansion coefficient: $\alpha$ | 1.64 $10^{-5}$ [1/K] |

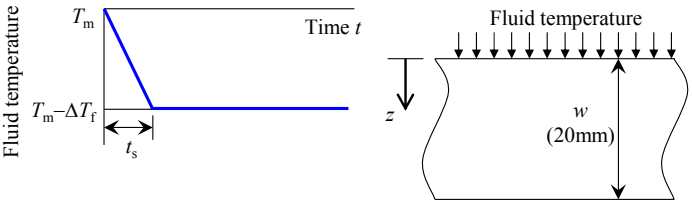


Figure 7. Analyzed model for thermal loading caused by linear change in fluid temperature.

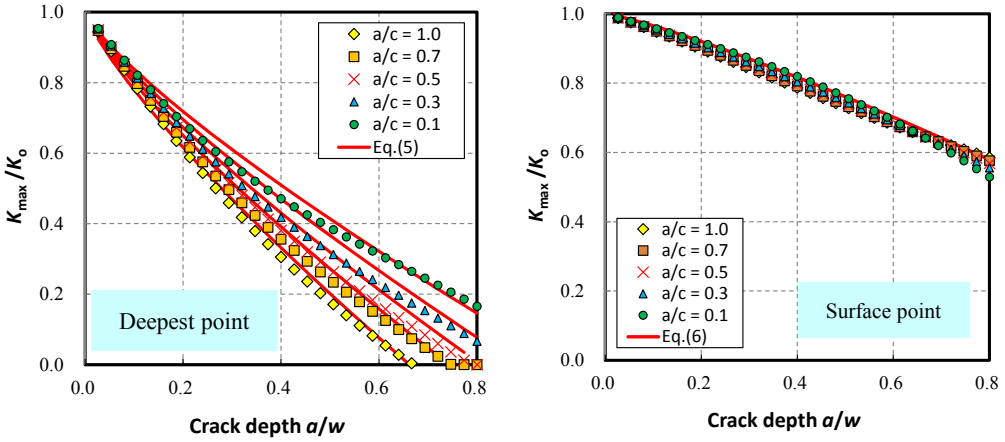


Figure 8. Change in the maximum stress intensity factor normalized by $K_o$ for various $a/c$ values and $K_{max}/K_o$ values predicted by Eqs. (5) and (6) ($H$ = 5,000 W/m$^2$K, $t_s$ = 1,000 s).

The crack growth prediction was made using the crack growth rate for stainless steels in air environment prescribed in the JSME (Japan Society of Mechanical Engineers) FFS code (JSME, 2012), which is referred to as FFS growth rate. The FFS growth rate for fully-reversed load is given by:

$$V_{(\mathrm{JSME})}\left[\mathrm{m/cycle}\right]=10^{H}\times 18.61\times 10^{-3}\left(\Delta K\left[\mathrm{MPa}\sqrt{\mathrm{m}}\right]\right)^{3.3} \tag{3}$$

where $H$ is the constant determined by the temperature and $H$ = –9.95 for 25°C was used. The DFC was estimated by crack growth prediction using the growth rate of $V_{(\mathrm{JSME})}$ × 2.4. Figure 6 shows the estimated fatigue life $N_p$ and DFC. The initial depth of $a_i$ = 300 μm gives good estimation, although $a_i$ = 50μm was applied for predicting the fatigue life obtained by the fatigue tests. The increase in the initial depth corresponds to the margins for the initiation. Thus, the fatigue damage assessment using CUF is replaced with the crack growth prediction using $a_i$ = 300 μm and growth rate of $V_{(\mathrm{JSME})}$ × 2.4.

## FATIGUE ASSESSMENT FOR THERMAL LOADING

The PFT concept was applied to the fatigue caused by temperature transients, which are the main source of fatigue damage for nuclear power plant components. To draw the P-curve for the thermal loading, the crack growth was predicted for the model shown in Figure 7. The fluid temperature was assumed to decrease linearly from $T_m$ to $T_m-\Delta T_f$ with a transient time of $t_s$. The change in the stress in the depth direction can be obtained analytically (Jones and Lewis, 1995; Kamaya, 2014a) and the stress intensify factor for a semi-elliptical crack on a plate, having a thickness $w$ of 20 mm, was obtained using the weight function method (Shen and Glinka, 1991). The stress intensify factors were calculated assuming the stainless steel constants shown in Table 3. Then, the maximum stress intensify factor $K_{max}$ was calculated during the thermal transient. Figure 8 shows the $K_{max}$ normalized by $K_o$, which is defined by:

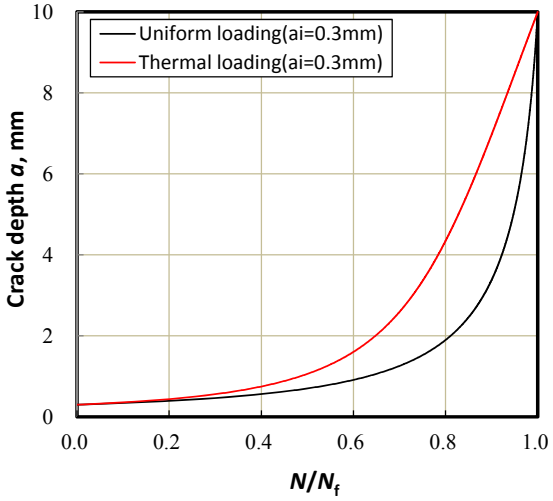


Figure 9. Crack growth curves (P-curves) obtained assuming initial depth of $a_i$ = 300 μm and $a/c$ = 1

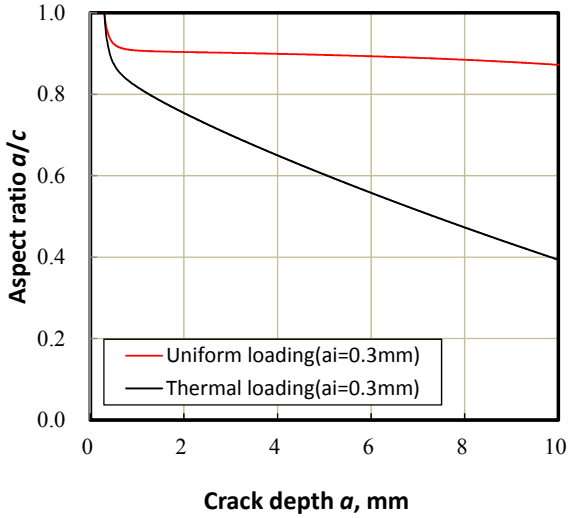


Figure 10. Changes in aspect ratio during fatigue crack growth prediction.

$$K_o = f\sigma_{\max(z=0)}\sqrt{\pi a} \tag{4}$$

where $\sigma_{\max(z=0)}$ is the maximum stress at the surface. $K_o$ corresponds to the stress intensity factor obtained for a uniform stress having a magnitude of $\sigma_{\max(z=0)}$. $K_{\max}$ is identical to $K_o$ regardless of the crack depth for a uniform cyclic stress. The decrease in $K_{\max}/K_o$ with crack depth indicates the crack growth deriving force decreases as the crack deepens.

The change in $K_{\max}/K_o$ with the normalized crack depth $a/w$ did not depend on fluid temperature range $\Delta T$ and thermal conductivity and it was almost the same for various heat transfer coefficients $H$ and transient times $t_s$ (Kamaya, 2017), while the values of $H$ = 5,000 W/m$^2$K and $t_s$ = 1,000 s were applied for Figure 8. The $K_{\max}/K_o$ at the deepest point depended on crack shape $a/c$, while almost the same $K_{\max}/K_o$ was obtained at the surface point. In order to predict the change in $K_{\max}/K_o$ with crack depth, the following equations have been proposed by Kamaya (2017).

$$\frac{K_{\max}}{K_o} = 1 - \left(0.41\frac{a}{c} + 0.98\right)\left(\frac{a}{w}\right)^{0.8} \quad \text{(For the deepest point)} \tag{5}$$

$$\frac{K_{\max}}{K_o} = 1 - 0.55\left(\frac{a}{w}\right)^{1.2} \quad \text{(For the surface point)} \tag{6}$$

These equations provide almost the upper bound of the analysed value.

Growth of a surface crack was simulated for thermal and uniform loadings using the growth rate of $V_{(JSME)} \times 2.4$. The $\Delta K$ was calculated as $\Delta K = 2K_{\max}$ considering a reversed load caused by a trapezoidal waveform of the fluid temperature fluctuation (Kamaya, 2014b). The depth of $a_i$ = 300 μm and aspect ratio of $a/c$ = 1.0 were assumed as initial conditions. $\Delta K$ was calculated for every 5 μm of growth in the depth direction. Then, the growths in the surface and depth directions were calculated.

Figure 9 shows the change in crack depth with the normalized number of cycles $N/N_f$. These P-curves were not dependent on $\Delta T$ and strain range and less dependent on heat transfer coefficients and transient time $t_s$. Moreover, the curves did not depend on the proportionality constant in the crack growth equation, which is $10^H \times 18.61 \times 10^{-3}$ in Equation 3. The type of loading (thermal or uniform loading) and the exponential constant in the crack growth equation, which is 3.3 in Equation 3, affect the P-curve shape. The crack growth curve for the thermal loading was more moderate, which means that the curve inclination

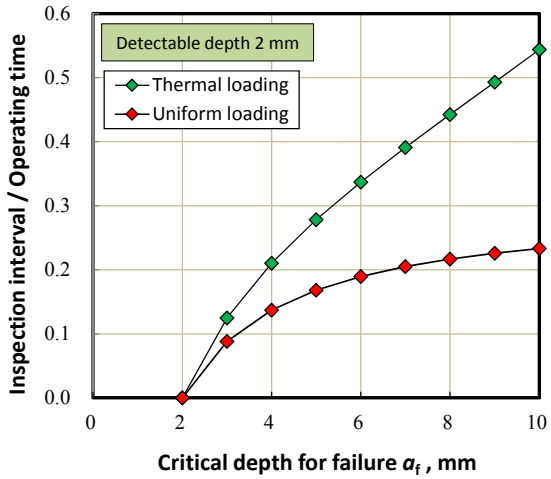


Figure 11. Intervals before the next inspection predicted from the P-curve.

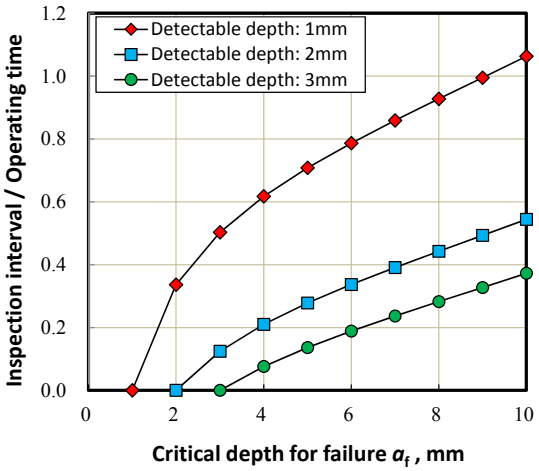


Figure 12. Intervals before the next inspection predicted from the P-curve for various detectable crack depths (thermal loading).

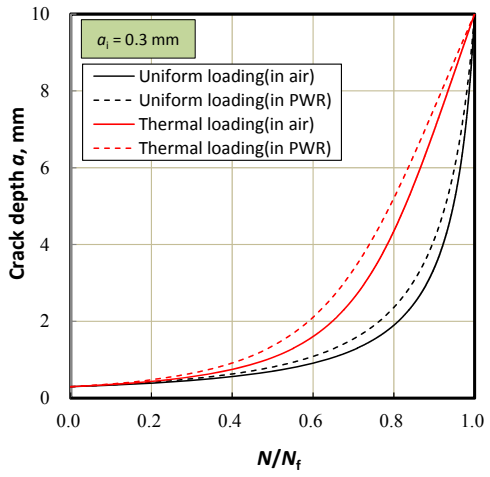


Figure 14. P-curves obtained for air and PWR water environments assuming initial depth of $a_i$ = 300 μm and $a/c$ = 1.

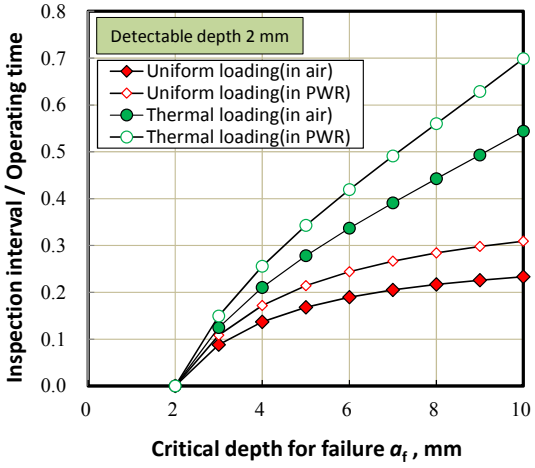


Figure 15. Intervals before the next inspection predicted from the P-curves for air and PWR water environments.

at the end of fatigue life was relatively small. Therefore, as shown in Figure 5, the residual life secured after an inspection was longer for the thermal loading than that for the uniform loading.

The change in aspect ratio during the crack growth is shown in Figure 10. The difference in the aspect ratio was significant between the thermal and uniform loadings. The aspect ratio for the uniform loading was about 0.9 for a well-developed semi-elliptical surface crack. The aspect ratio for the thermal loading was close to that of the uniform loading when the crack depth was small. However, it decreased as the crack depth increased because the growth in the depth direction was suppressed due to the stress gradient.

In the flaw tolerance assessment, the interval before the next inspection is determined from the crack growth prediction. The component can be used only while a postulated crack does not exceed the allowable crack size determined by FFS assessment. In the PFT concept, the interval is determined as the residual life obtained by the P-curve as noted in Figure 5. The interval depends on the detection capability of the inspection technique and the crack growth curve (P-curve). Additionally, the operating period before

the inspection is an important factor for determining the interval. Since the ordinate of the P-curve is expressed by $N/N_f$, a longer operation time results in a longer interval. Then, in Figure 11, the inspection interval was calculated assuming the detectable crack depth to be 2 mm. The inspection interval varied depending on the critical depth for failure $a_f$. In the case of thermal loading and $a_f$ = 10 mm, the interval before the next inspection was more than 20 years if the plant has been operated more than 40 years. The interval became about 9 years for uniform loading. Figure 12 shows the interval for thermal loading for various detectable crack sizes. A smaller detectable size resulted in a longer interval. A longer operation time before reaching CUF = 1 meant a smaller strain amplitude. A smaller crack depth at CUF = 1 implied less strain amplitude. The PFT allowed the operating experience (plant performance) to be reflected onto the future inspection program.

## EFFECT OF PWR WATER ENVIRONMENT

The P-curve and inspection interval were calculated assuming fatigue crack growth in the PWR water environment. The JSME FFS code (2012) prescribes the fatigue growth rate in the PWR water environment of 325°C for a fully reversed load with the rise time of 1000 s as:

$$V_{(\mathrm{JSME\_PWR})}\left[\mathrm{m/cycle}\right] = 5.513\times10^{-11}\left(\Delta K\left[\mathrm{MPa}\sqrt{\mathrm{m}}\right]\right)^{3.0} \tag{7}$$

It has been shown that the reduction in the fatigue life in the PWR water environment is brought about not by the enhanced crack initiation but by accelerated crack growth (Kamaya, 2013b). The reduction in the fatigue life could be estimated by considering an accelerated crack growth rate assuming the same initial depth (Kamaya, 2013b). Then, the P-curve for the PWR water environment was calculated using the accelerated growth rate, which corresponded to Equation 7, assuming the same initial depth of $a_i$ = 300 μm. Figures 14 and 15 show the P-curves and intervals before the next inspection, respectively. The P-curves were more moderate for the PWR water environment. It should be noted again that the P-curve shape depends only on the exponential constant, which is 3.0 in Equation 7. Therefore, the curve shape difference between the air and PWR water environments emanated from the difference in the exponential constant. The smaller exponential constant (3.0) than that for air (3.3) caused moderate crack growth. The interval before the next inspection became longer for the PWR water environment.

## CONCLUSION

In this study, a concept of performance based flaw tolerance (PFT) was proposed in order to achieve a reasonable flaw tolerance assessment considering operating experience. The longer operating time and smaller crack growth before the inspection allow a longer interval before the next inspection. To apply the PFT concept, the fatigue assessment using the CUF was replaced with the crack growth prediction. The allowable number of cycles prescribed by the DFC was successfully predicted by the crack growth assuming an initial depth of $a_i$ = 300 μm and an accelerated growth rate considering a structural margin of 2.4. Then, the postulated crack growth curve (P-curve) was derived for the uniform and thermal loading conditions. Use of the P-curve made it possible to show the interval before the next inspection from the operating time before the inspection, detectable crack size of the inspection technique and critical size. It was demonstrated that this concept is applicable to the fatigue assessment in the PWR water environment.

## REFERENCES

ASME. (2015a). *Rules for Inservice Inspection of Nuclear Power Plant Components – ASME Boiler and Pressure Vessel Code Section XI*, ASME, New York, USA.

ASME. (2015b). *Rules for Construction of Nuclear Facility Components – ASME Boiler and Pressure Vessel Code Section III*, ASME, New York, 2015.

Chopra, O. K. and Shack, W. J. (2007). "Effect of LWR coolant environments on the fatigue life of reactor materials", NUREG/CR-6909, ANL-06/08.

Colin, J. and Fatemi, A. (2010). "Variable amplitude cyclic deformation and fatigue behavior of stainless steel 304L including step, periodic, and random loading", *Fatigue & Fracture of Engineering Materials & Structures*, 33, 205-220.

Gilman, T. D., Alleshwaram, A. and Satyan-Sharma, T. (2015). "Industry's first NRC approved appendix L flaw tolerance evaluation to manage fatigue in a surge line", P*roceedings of the ASME 2015 Pressure Vessels and Piping Conference*, ASME, Boston, MA, paper no. 97851.

Gosselin, S. R., Simonen, F. A., Heasler, P. G. and Doctor S. R. (2007). "Fatigue crack flaw tolerance in nuclear power plant piping - A basis for improvements to ASME Code Section XI Appendix L", NUREG/CR-6934.

Jaske, C. E. and O'Donnell, W. J. (1977). "Fatigue design criteria for pressure vessel alloys", *ASME Journal of Pressure Vessel Technology*, 99, 584-592.

Jones, I. S. and Lewis, W. J. (1995). "The effect of various constraint conditions in the frequency response model of thermal striping", *Fatigue & Fracture of Engineering Materials & Structures*, 18, 489-502.

JSME. (2012). *Codes for Nuclear Power Generation Facilities: Rules on Fitness-for-service for Nuclear Power Plants JSME S NA1-2012*, Japan Society of Mechanical Engineers, Tokyo, Japan.

Kamaya, M. (2013a). "Damage assessment of low-cycle fatigue by crack growth prediction (fatigue life under cyclic thermal stress)", *Transactions of the Japan Society of Mechanical Engineers*, A79, 1530-1544.

Kamaya, M. (2013b). "Environmental effect on fatigue strength of stainless steel in PWR primary water – Role of crack growth acceleration in fatigue life reduction", *International Journal of Fatigue*, 55, 102-111.

Kamaya, M. (2014a). "Assessment of thermal fatigue damage caused by local fluid temperature fluctuation (Part I: Characteristics of constraint and stress caused by thermal striation and stratification)", *Nuclear Engineering and Design*, 268, 121-138.

Kamaya, M. (2014b). "Assessment of thermal fatigue damage caused by local fluid temperature fluctuation (Part II: Crack growth under thermal stress)", *Nuclear Engineering and Design*, 268, 139-150.

Kamaya, M. (2017). "Fatigue crack tolerance design for stainless steel by crack growth analysis", *Engineering Fracture Mechanics*, 177, 14-32.

Kamaya, M. and Kawakubo, M. (2012a). "Strain-based modeling of fatigue crack growth – An experimental approach for stainless steel", *International Journal of Fatigue*, 44, 131-140.

Kamaya, M. and Kawakubo, M. (2012b). "Damage assessment of low-cycle fatigue by crack growth prediction (development of growth prediction model and its application)", *Transactions of the Japan Society of Mechanical Engineers*, A78, 1518-1533.

Kamaya, M. and Kawakubo, M. (2015). "Mean stress effect on fatigue strength of stainless steel", *International Journal of Fatigue*, 74, 20-29.

Kamaya, M. and Nakamura, T. (2013). "A flaw tolerance concept for plant maintenance using virtual fatigue crack growth curve", *Proceedings of the ASME 2013 Pressure Vessels and Piping Conference*, ASME, Paris, France, paper no. 97851.

Kawakubo, M. and Kamaya, M. (2011). "Fatigue life prediction of stainless steel under variable loading (damage factors determining fatigue life and damage evaluation for two-step test)", *Journal of the Society of Materials Science, Japan*, 60, 871-878.

Nakamura, T., Iwasaki, M. and Asada, S. (2007). "Optimization of Environmental Fatigue Evaluation: Step 1", P*roceedings of the ASME 2007 Pressure Vessels and Piping Conference*, ASME, San Antonio, TX, paper no.26247.

Rothenhöfer, H. and Manke, A. (2013). "Monitoring with good cause – Basic principles and current status", *Proceedings of the ASME 2013 Pressure Vessels and Piping Conference*, ASME, Paris, France, paper no. 97029.

Shen, G. and Glinka, G. (1991). "Weight functions for a surface semi-elliptical crack in a finite thickness plate", *Theoretical and Applied Fracture Mechanics*, 15, 247-255.